IBM Research Report

Tunneling Spectroscopy of Two-State Systems

J. A. Gupta, C. P. Lutz, A. J. Heinrich, D. M. Eigler
IBM Research Division
Almaden Research Center
650 Harry Road
San Jose, CA 95120-6099

Research Division
Almaden - Austin - Beijing - Haifa - India - T. J. Watson - Tokyo - Zurich

Tunneling Spectroscopy of Two-State Systems

J.A. Gupta, C.P. Lutz, A.J. Heinrich and D.M. Eigler

IBM Research Division, Almaden Research Center, 650 Harry Rd, San Jose, CA 95120

Abstract

We observe gap-like and negative differential resistance features in tunneling spectra resulting from transitions between states of H_2 in the junction of a low-temperature scanning tunneling microscope. We develop a model for the conductance of a saturable two-state system where transitions are driven by inelastic scattering of tunneling electrons that explains the distinctive lineshapes of these spectral features and can provide information on the residence times in each state.

In the emerging field of molecular electronics (*1*), two-terminal measurements with scanning tunneling microscopes (STMs) enable study of the electronic properties of single molecules and atoms in a controlled environment. Such studies have revealed that electronic transport on the atomic scale can strongly depend on atomic or molecular motion (*2-3*), resonant tunneling through localized states (*4*), and molecular conformation changes (*5*).

Here we study tunnel junctions comprising an STM tip, a flat metal surface, and H_2 molecules. Within a range of H_2 surface coverage, differential conductance (*dI/dV*) spectra reveal gap-like and negative differential resistance (NDR) features. By directly resolving two-state noise in the tunnel current, we can attribute these features to transitions between states of H_2 that are driven by inelastic scattering of tunneling electrons. The threshold voltages for transitions increase with H_2 coverage, depend on tip-sample separation and do not match known rotational or vibrational modes. We develop a model for a two-state system where the excited state is reached by inelastic scattering and has a sufficiently long lifetime that an associated elastic conductance is measured by subsequent tunneling electrons. The model reproduces both gap-like and NDR features and can provide information on inelastic channel strengths and residence times even in cases where direct resolution of two-state noise is limited by instrumental bandwidth.

Experiments were performed using ultra-high vacuum STMs operating at temperatures of *T*=5K and 2.5<*T*<18K. In this temperature range, *dI/dV* spectra remain qualitatively unchanged. Data presented here were taken at *T*=5K. Clean surfaces of single-crystal Cu(111) were prepared by Ar sputtering and annealing to 600ºC. After transferring the Cu crystal to the cold STM, the polycrystalline Ir tip was positioned over a clean terrace and *dI/dV* spectra were recorded with a lock-in amplifier by adding a modulation to the sample voltage *V*. H_2 gas was then admitted to the room-temperature UHV chamber (P_{H2}~1E-8 Torr) through a leak valve, producing a constant flux of H_2 cryopumped by the low-temperature section containing the STM. Because direct line-of-sight to the surface was blocked by a mechanical shutter held at *T*=5K, we expect the H_2 to be cold prior to adsorption. Previous studies indicate that H_2 is only weakly bound to cold, noble metal surfaces by van der Waals forces (physisorption) (*6,7*).

Figure 1(a) shows the evolution of dI/dV spectra that occurs with H_2 exposure. Spectra taken with <870min exposure are unchanged from the clean Cu surface. A gap-like feature then suddenly appears with conductance peaks at V_{gap}=80mV that are symmetric about V=0 [Fig. 1(b)]. Figure 1(a) shows that V_{gap} increases and the conductance peaks broaden with increasing H_2 exposure, until the gap-structure loses visibility for V_{gap}>200mV. With additional exposure, a feature exhibiting negative differential resistance emerges [Figs. 1(a,c)]. Dips in dI/dV first occur at V_{ndr} =20mV before broadening and shifting toward higher voltage in a similar fashion to the gap-like feature.

Owing to the mobility of physisorbed H_2, we are unable to directly observe single H_2 molecules in our STM images, making it difficult to estimate the surface coverage as a function of exposure. For long exposures (> 2000min), STM images reveal ordering of H_2 beginning around surface adsorbates and step edges that is incommensurate with the underlying Cu lattice. The ordered layer eventually grows to cover entire terraces; by this time the gap-like and NDR features have broadenend and shifted considerably (V_{gap} > 200mV, V_{ndr} > 75mV), leaving unchanged the small dip at V=0 that is visible in Fig. 1(c). Based on comparable overlayers of physisorbed rare gases (8), it is likely that gap-like and NDR features occur at sub-monolayer H_2 coverage.

Conductance spectra depend on the tip-sample separation, which can be parametrized by the junction resistance R (decreasing R by one decade moves the tip ~0.1nm closer to the surface). For these measurements, we stabilized the H_2 coverage by closing the leak valve when the gap-like feature first becomes visible. V_{gap} continues to shift at a reduced rate for several hours afterwards, but eventually settles to a constant value. Figure 2(a) shows that while only the gap-like feature is visible at R > 20MΩ, NDR emerges for R < 10MΩ, so that both features can occur in the same spectrum. Data taken at R=10MΩ during the course of Fig. 1 indicate that the NDR and gap-like features appear concurrently with H_2 exposure. This suggests that tip proximity to the surface and higher coverage both enable the transition responsible for the NDR feature. V_{ndr} and V_{gap} are typically constant for 1MΩ < R < 1GΩ, but shift toward low voltage for R < 1MΩ [Fig. 2].

There is often noise present in the conductance peaks of the gap-like feature that provides information on the transition occurring at V_{gap}. We can directly resolve this noise in the tunnel current by turning off the voltage modulation and holding the tip-sample separation constant. Fig. 3(a) demonstrates that the noise results from repeated switching between two states. The system resides in a ground state for $V < V_{gap}$ and an excited state for $V > V_{gap}$. For $V \sim V_{gap}$, either state is occupied with equal probability. The conductances of ground (σ_0) and excited (σ_1) states are independent of voltage, indicating that nonlinearities in *dI/dV* solely result from the switching behavior. We calculate the probability of residence (n_0,n_1) in each state at a given voltage using the relations:

$$\bar{\sigma} = n_0\sigma_0 + n_1\sigma_1 \tag{1}$$

$$n_0 + n_1 = 1, \tag{2}$$

where $\bar{\sigma}$ is the time-averaged conductance. The coincidence of V_{gap} with changes in $n_1(V)$ [Fig. 3(b)] indicates that conductance peaks occur as the predominant state of the system changes from the ground to excited state.

To learn more about the mechanism for transitions, we studied the residence times in ground (t_0) and excited (t_1) states as a function of current by compiling histograms of residence probability versus time [Fig. 3(c)]. The probability distribution can be well fit by a single exponential whose decay constant is the residence time. The dependence of residence times on current in Fig. 3(c) shows that the transition rates between states increase proportionately with the number of available tunneling electrons. This suggests that transitions are driven by inelastic scattering, which is also consistent with the symmetry of *dI/dV* spectra about $V=0$.

The tunneling current through a junction that can switch between two states is the sum of contributions from elastic and inelastic conductance channels. We assume that the tip and sample densities of states are constant over the voltage range of interest. Inelastic conductance channels transfer the junction from state *0* to state *1* with conductance σ_{01} or vice versa (σ_{10}), provided that the sample voltage exceeds threshold values V_{01} and V_{10} respectively [Fig. 4(a), inset]. If we exclude spontaneous excitation into state *1*, the tunneling current is:

$$I(V) = \left(n_0\sigma_0 + n_1\sigma_1\right)V + \left(n_0\sigma_{01}(V - V_{01}) + n_1\sigma_{10}(V - V_{10})\right) \quad \text{for } V \geq V_{01}, \qquad (3)$$

$$I(V) = \sigma_0 V \qquad\qquad\qquad\qquad\qquad\qquad\qquad \text{for } V < V_{01}.$$

For clarity, we consider only $V \geq 0$ with the understanding that $I(V)$ should be antisymmetric about $V=0$. The residence probability in the excited state is:

$$n_1 = \frac{\Gamma_{01}}{\Gamma_{01} + \Gamma_{10}} = \frac{\sigma_{01}(V - V_{01})}{\sigma_{01}(V - V_{01}) + \sigma_{10}(V - V_{10}) + eS_{10}} \quad \text{for } V \geq V_{01}, \qquad (4)$$

$n_1 = 0$ for $V < V_{01}$.

Here Γ's represent the total transition rates between states 0 and 1, and S_{10} is the spontaneous relaxation rate from state 1. After substitutions using Eqs. 2 and 4, differentiation of Eq. 3 gives an expression of the form:

$$dI/dV = A + \frac{B}{\left(1 + (V - V_{01})/V^*\right)^2} \quad \text{for } V \geq V_{01}, \qquad (5)$$

$dI/dV = \sigma_0$ for $V < V_{01}$,

where A, B and V^* are voltage-indpendent functions of the seven parameters in the model: $\sigma_0, \sigma_1, \sigma_{01}, \sigma_{10}, V_{01}, V_{10}, S_{10}$ (9). Figure 4(a) shows that Eq. 5 produces a gap-like feature with conductance peaks at $V=V_{01}$ when $\sigma_1 > \sigma_0$. V^* sets the decay of dI/dV from the extremum at $V=V_{01}$, A is equal to the asymptotic conductance as $V \to \infty$ and the sum $A+B$ is equal to the conductance at $V=V_{01}$. Eq. 5 instead produces dips in dI/dV when $\sigma_0 > \sigma_1$ (5,10). Although transition rates are usually faster than can be resolved with the STM, two-state noise has been measured at V_{ndr}, verifying that the NDR feature results from switching where $\sigma_0 > \sigma_1$. Such noise can emerge at low junction resistance [e.g. R=100kΩ in Fig. 2(a)], indicating that very close proximity to the surface may act to decrease transition rates.

The sharp onset and more gradual decay of the peaks/dips in dI/dV spectra can be physically understood as a saturation effect. When increasing V from zero bias, an inelastic path becomes available at $V = V_{01}$, suddenly increasing n_1 and thus producing a change in dI/dV. For $V > V_{01}$, dI/dV decreases from the extremal value as dn_1/dV approaches zero. The model may also be applicable to a previous study of NDR where a similar lineshape was observed (5); a host of other spectral features are possible

5

depending on choices of model parameters. In the limit that $\Gamma_{10} \gg \Gamma_{01,}$ Eq. 5 reduces to conventional inelastic electron tunneling spectroscopy, where residence in an excited vibrational state is negligible under typical conditions.

It is necessary to introduce broadening to Eq. 5 in order to fit the experimental data. Sources of broadening may include intrinsic uncertainty in the excitation energy eV_{01} and dynamic fluctuations in local coverage due to the mobility of physisorbed H_2. Because these sources are difficult to quantify, we empirically convolve Eq. 5 with a Gaussian distribution about V_{01}. The choice of standard deviation is based on matching the transition region just below V_{01}, as this region is infinitely sharp in the model. We treat gap-like and NDR features as independent two-state systems, assigning V_{01} to either V_{gap} or V_{ndr} as required.

Figure 3(b) includes a calculated *dI/dV* curve chosen to fit the experimental data (*11*). While agreement between calculation and data is good, we note that *dI/dV* data alone cannot constrain all seven parameters. Because transition rates are slow compared to rates for elastic tunneling, the parameters S_{10}, σ_{10}, and σ_{01} are not uniquely determined and can only be constrained by measurements of t_1 and t_0 from two-state noise (*12*). The curve for $n_1(V)$ in Fig. 3(b) was calculated using identical parameters from the fit to *dI/dV*. The saturation of n_1 near unity indicates that the inelastic conductance channel σ_{10} is weak compared to σ_{01}.

We usually find that identical fits to *dI/dV* data can be produced with or without σ_{10}. Thus it is primarily through analysis of residence times [e.g. Fig. 3(c)] that the existence of σ_{10} is inferred. When two-state noise is not visible due to transition rates that exceed the instrumental bandwidth, it is difficult to determine whether relaxation from the excited state is inelastically driven or spontaneous. If we assume the latter dominates in these cases and set $\sigma_{10} = 0$, we obtain simpler expressions for *A*, *B* and V^*:

$$A = \sigma_1 \,,\, B = \left(V_{01}/V^* - 1\right)\left(\sigma_1 - \sigma_0\right) + \sigma_{01} \,,\, \text{with } V^* = eS_{10}/\sigma_{01} = e/(\sigma_{01}\,t_1). \tag{6}$$

If σ_{01} is much smaller than the first term in *B*, fits to *dI/dV* using Eq. 6 only yield the ratio S_{10}/σ_{01}. This is typically the case for NDR data [Fig. 4(b)]. Transition rates well outside the instrumental bandwidth can also occur at V_{gap}. The fit in Fig. 4(c) is such that σ_{01} is comparable to the first term in *B*, so that σ_{01} and S_{10} are uniquely determined,

giving an excited state residence time of $1/S_{10}=t_1=2.2$ns. While it is unclear if the assumption $\sigma_{10}=0$ is justified for these data, this example illustrates that the model can provide information on residence times even when two-state noise is not directly resolved.

In Ref. (*5*), NDR resulted from changes in molecular conformation states effected by inelastic excitation of vibrational modes. Previous studies have measured the H-H stretch at 510meV for physisorbed H_2 and 464meV for H_2 chemisorbed at step edges on Cu(510) (*13*). Rotational transitions occur at 45/73meV for physisorbed para/ortho-H_2 and 31/61meV for chemisorbed para/ortho-H_2 (*13*). Vibrations of H_2 in the physisorption potential well on Cu(100) occur at 9meV (*7*). In ~20 independent repetitions starting with a clean Cu surface, V_{gap} begins in the range 25-90mV before shifting to $V_{gap}>200$mV with increased coverage. V_{ndr} more reliably begins at 11 ± 2mV and shifts to $V_{ndr}>75$mV. Similar values were observed for HD and D_2, although it is difficult to establish whether small isotope shifts occur. While some of the rotational or vibrational modes fall within these ranges of values, it is unlikely that such modes would exhibit the variability or the dependence on coverage observed here.

Conductance measurements of single H_2 molecules in the point contact regime have revealed a longitudinal vibrational mode at 64meV for H_2 bound between Pt electrodes (*14*). While we cannot rule out possible correspondence with V_{gap}, we note that the contact geometry and electrode separation are quite different in our STM measurements. We instead speculate that the gap-like and NDR features reflect transitions of H_2 between different binding sites at the tip apex [Fig. 4(d)]. Experiments and total energy calculations indicate that H_2 chemisorption is favorable at the low-coordination sites of step edges, with potential well depths less than 100meV for Cu(510) (*13,15*). This suggests that stable binding of H_2 to low-coordination sites on the tip may be possible. We find that the shape and position of gap-like and NDR features can significantly change when the atomic structure at the tip apex is perturbed, which may explain the variability of gap-like and NDR features. The identity of atoms at the tip apex is generally unknown, though we expect that tip-preparation via contact with the surface results in a transfer of surface atoms to the tip apex. We have also observed NDR features on Cu(001), Ni(110), CO/Cu(111), NiAl(110), Pt(111), Ag(111) and on Cu(111) with a

tip terminated by a CO molecule. However, gap-like features have only been found on Cu(001) and Al_2O_3/NiAl(110), suggesting that the gap-like feature is more dependent on the identity of atoms at the tip apex. The shifts of V_{gap} and V_{ndr} with coverage may be qualitatively explained as molecular motion that is hindered by surrounding physisorbed H_2. The number of molecules involved in the switching is difficult to estimate, although the atomic dimensions of the tunnel junction likely limit this number to a few at most.

We conclude by noting that the data in Fig. 4(c) could readily be mistaken for the quasiparticle excitation spectrum in a BCS superconductor. The results presented here demonstrate that a variety of lineshapes can result simply from inelastically driven transitions in two-state systems, providing opportunities for tailored transport characteristics in potential molecular electronic devices.

References

1. J.R. Heath and M.A. Ratner, Phys. Today **56**, 43 (2003).

2. D.M. Eigler, C.P. Lutz and W.E. Rudge, Nature **352**, 600 (1991).

3. B.C. Stipe, M.A. Rezaei and W. Ho, Phys. Rev. Lett. **81**, 1263 (1998).

4. I.-W. Lyo and Ph. Avouris, Science **245**, 1369 (1989).

5. J. Gaudioso, L.J. Lauhon and W. Ho, Phys. Rev. Lett. **85**, 1918 (2000).

6. S. Andersson and J. Harris, Phys. Rev. Lett. **48**, 545 (1982).

7. K. Svensson and S. Andersson, Phys. Rev. Lett. **78**, 2016 (1997).

8. F. Brunet et al., Surf. Sci. **512**, 201 (2002); J. Park et al., Phys. Rev. B **60**, 16934 (1999).

9. $A = \left(\sigma_{01}(\sigma_1 + \sigma_{10}) + \sigma_{10}(\sigma_0 + \sigma_{01})\right)/(\sigma_{01} + \sigma_{10})$

$$B = \frac{\sigma_{01}\left[(\sigma_{01}V_{01} + \sigma_{10}V_{10} - eS_{10})(\sigma_1 - \sigma_0) + 2\sigma_{01}\sigma_{10}(V_{01} - V_{10}) + eS_{10}(\sigma_{01} - \sigma_{10})\right]}{\left(\sigma_{10}(V_{01} - V_{10}) + eS_{10}\right)(\sigma_{01} + \sigma_{10})}$$

$$V^\dagger = \left(\sigma_{10}(V_{01} - V_{10}) + eS_{10}\right)/(\sigma_{01} + \sigma_{10})$$

10. An NDR feature may also be produced when $\sigma_1 > \sigma_0$ if $n_1 \neq 0$ for $V < V_{01}$. In such a case, the inelastic channel σ_{10} acts to reduce the probability n_1 once $V > V_{10}$, thus switching from a high to low conductance state as required for NDR.

11. Fit parameters are: V_{01}=108mV, V_{10}=70mV, σ_0=8.6nA/V, σ_1=21nA/V, σ_{01}=8pA/V, σ_{10}=0.1pA/V, S_{01}=1000 s^{-1}, broadening = 4.7mV.

12. Additional studies of $t_1(V)$ indicate that t_1 increases for $V > V_{01}$, suggesting that other mechanisms not included in our model affect transition rates. Possibilties include electric field effects or interaction with surrounding H_2 molecules.

13. K. Svensson et al., Phys. Rev. Lett. **83**, 124 (1999).

14. R.H.M. Smit et al., Nature **419**, 906 (2002).

15. L. Bengtsson et al., Phys. Rev. B **61**, 16921 (2000).

16. We thank C.T. Rettner, A.F. Panchula and M.W. Hart for their help and acknowledge support from the Defense Advanced Research Projects Agency.
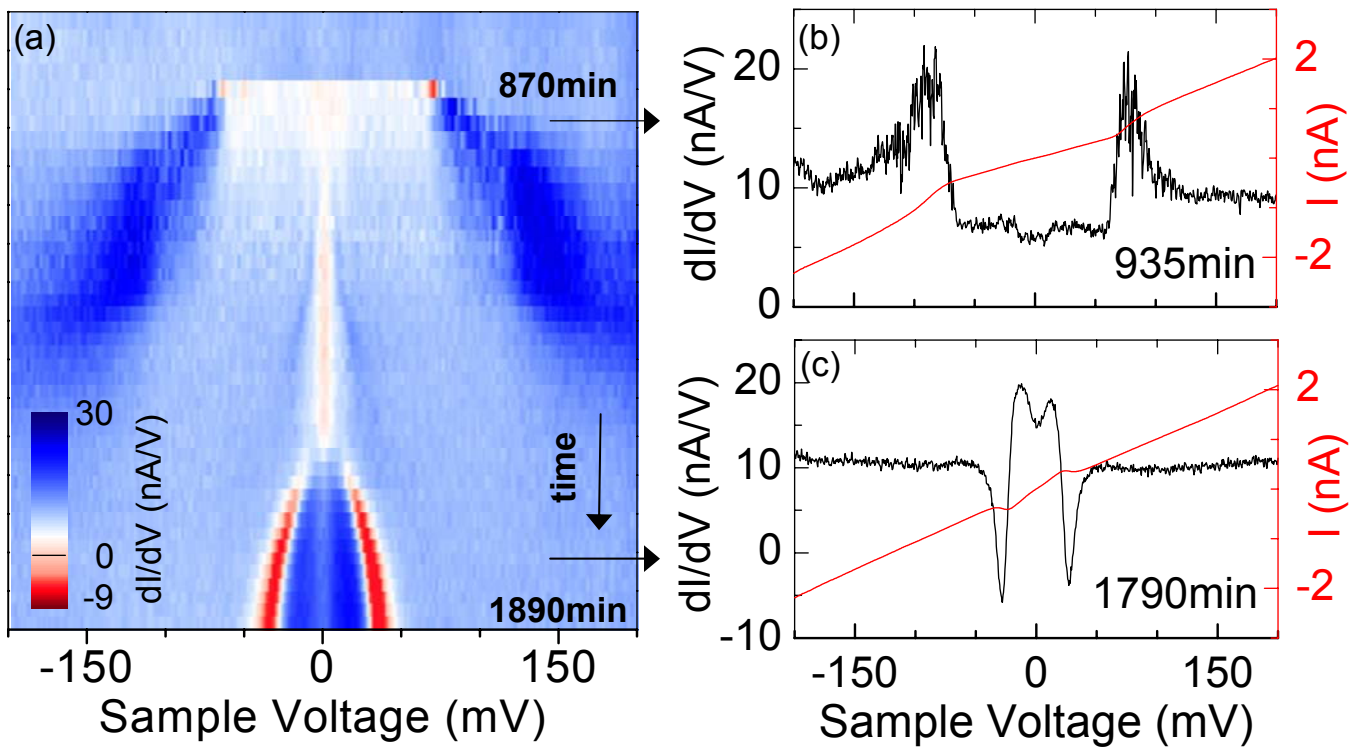
Fig. 1: (a) *dI/dV* spectra taken as H_2 coverage increases with time. (b),(c) Linecuts of *dI/dV* indicated by the arrows in (a). Shown in red are corresponding *I(V)* curves. *R* =100MΩ (*V*=100mV, *I*=1nA), modulation =0.5mV$_{rms}$. Spectra are the average of 10x1min sweeps.
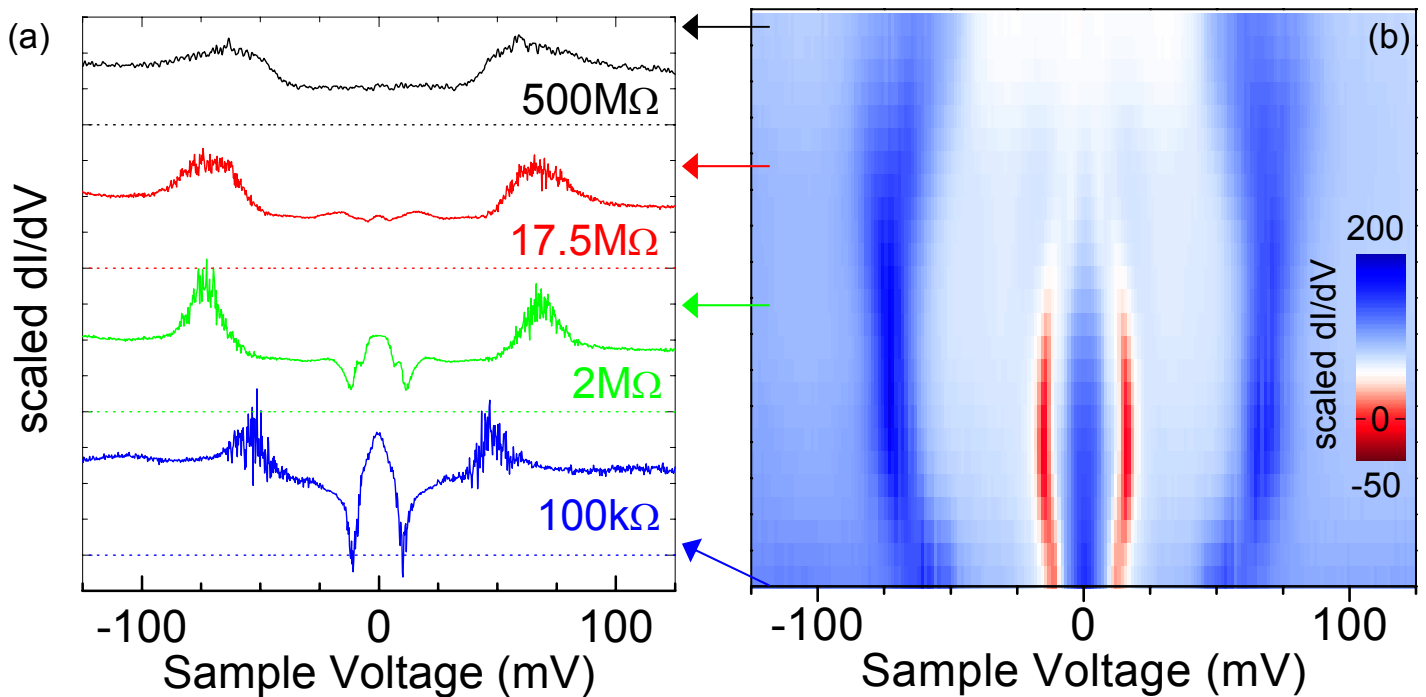
Gupta et al., Figure 1

Fig. 2: Emergence of NDR with decreasing junction resistance. All data are scaled by $R/10M\Omega$ (V=100mV, I=10nA). (a) Spectra are offset by 200nA/V for clarity. Dotted lines indicate zero conductance for each scan. Data at R=500MΩ are the average of 5 sweeps, while the others are single sweeps. From top to bottom, RMS modulation =2mV, 1mV, 0.5mV, 0.2mV. (b) Complete series for 500MΩ<R<0.1MΩ.

Gupta et al., Figure 2
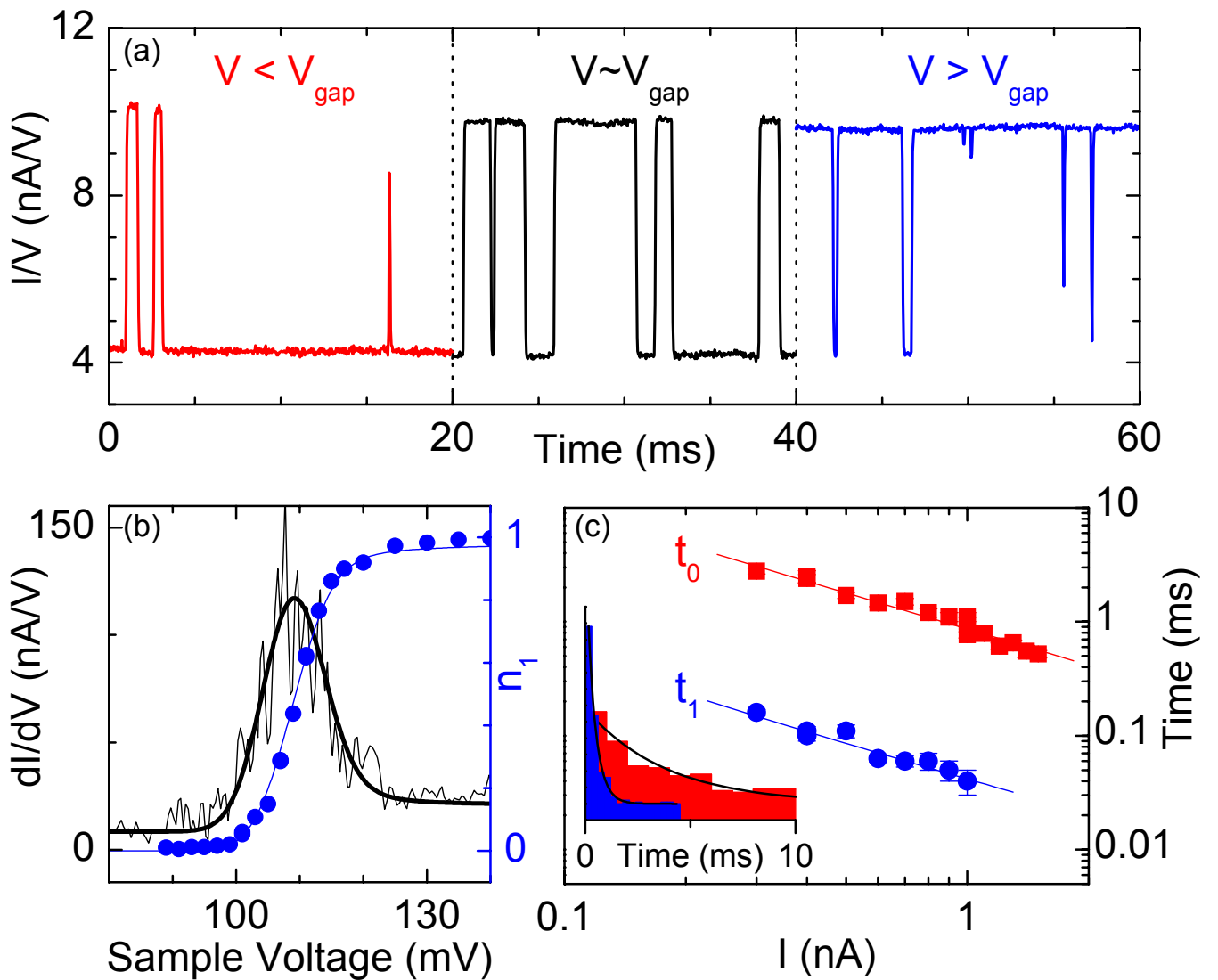
Fig. 3: Two-state noise at V_{gap}. (a) Switching in conductance with V=95mV (red), 109mV (black), 125mV (blue) taken after opening the STM feedback loop at V=150mV, I=1.5nA. (b) Left axis: dI/dV showing V_{gap}=108mV. The solid line is a fit using Eq. 5 and parameters in Ref. (11). Right axis (blue): Residence probability in the excited state. The solid line is calculated using Eq. 4 with identical parameters (11). (c) Inset: histogram of residence probability versus time for ground (red) and excited (blue) states extracted from two-state noise at V=110mV, I=0.2nA, along with exponential fits (black lines). Main (log-log scale): Residence times t_0 and t_1 from exponential fits. Lines are fits with slopes of -1.0. Data were taken shortly after those in (a-b), so that V_{gap}=120mV due to a higher coverage.

Gupta et al., Figure 3
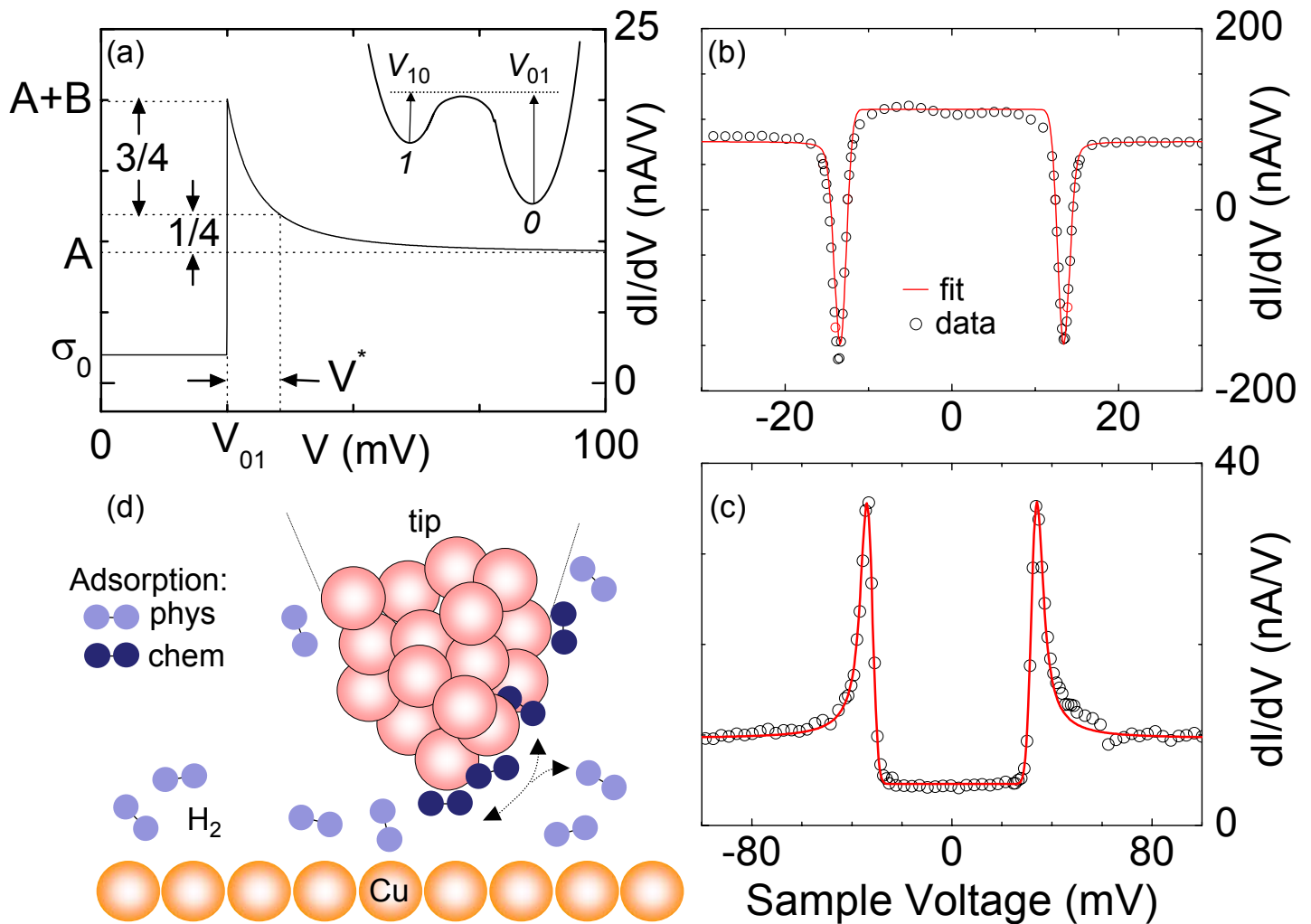
Fig. 4: Model and fits. (a) Calculation of *dI/dV* using Eq. 5 with σ_0=2nA/V, σ_1=10nA/V, σ_{01}=2nA/V, σ_{10}=0.5nA/V, S_{10}=0.1GHz, V_{01}=25mV, V_{10}=5mV. Inset: schematic of two-state system. (b) Data (open symbols) taken for H_2/Cu(111) with (*V*=10mV, *I*=1nA, 0.5mV$_{rms}$ modulation, 4 sweeps) and fit (red line) using Eq.6 with (σ_0 =110.8nA/V, σ_1 =74.1nA/V, V^*=0.03mV, V_{01}=13.3mV, broadening = 0.8mV). (c) Data (open symbols) taken for H_2/Cu(001) with (*V*=100mV, *I*=1nA, 0.5mV$_{rms}$ modulation, 20 sweeps) and fit (red line) with (σ_0 =4.5nA/V, σ_1 =9.7nA/V, σ_{01}=32.2nA/V, t_1=2.15ns, V_{01}=32.2mV, broadening =1.8mV). (d) Schematic of possible adsorption states at the tip apex.

Gupta et al., Figure 4